FINAL TECHNICAL REPORT

DoE Grant #DEFG0295ER54307

University of Maryland Account Numbers:
01527372, 01527373 (off campus) and 01527461

Project Titles:

High Resolution Spectroscopy in the Divertor and Edge Regions of Alcator-C Mod
and
Measurement of Radiative Transfer in Vacuum-UV Line Emission
from Magnetic Fusion Devices

REPORT

Spectroscopic diagnostics described below were carried out both at MIT and at the University of Maryland. At MIT, measurements were made of toroidal flow velocities in the mid-plane of the inner and outer scrape-off layers (SOL) of Alcator C-Mod plasmas, using a high-resolution spectrograph. Subsequently, the MIT/Alcator procedures based upon visible spectroscopy were transferred to the new Maryland centrifugal experiment (MCX). In a further effort towards data refinement, we expanded the hydrogen measurements from the $n \rightarrow 2$ Balmer series in the visible to the $n \rightarrow 1$ Lyman series in the vacuum-ultraviolet (vuv) spectral region. Recent results were presented at APS Division of Plasma Physics meetings and published in Physics of Plasmas in 2004 and 2005. Further details can be found in the annual progress reports to the Department of Energy.

ALCATOR EXPERIMENTS

At MIT, we performed measurements of toroidal flow velocities in the mid-plane of the inner and outer scrape-off layers (SOL) of Alcator C-Mod plasmas using a high-resolution spectrograph. Doppler shifts of the line emissions from either He^+ at 468.6 nm or neutral deuterium at 656.1 nm from two local gas jets were observed along radially-separated, toroidally-viewing chords to obtain the radial profiles of the toroidal ion and neutral flow velocities and of the temperatures in the mid-plane of the inner and outer SOL's. In these experiments, the ion vertical drift due to the toroidal magnetic field gradient (ion $B \times \nabla B$ drift) was directed towards the lower X-point, and an outer SOL plasma flow with a velocity in the range of 5 – 10 km/sec in the direction of the plasma current was observed at the mid-plane far above the divertor plates.

Plasma flow in a similar direction with similar velocities was observed in the inner SOL mid-plane. Interestingly, the neutral atoms in these views were observed to flow in the opposite directions in the inner and outer SOL's, i.e., the neutrals flow in the plasma current direction in the inner SOL and in the direction opposite to the plasma current in

the outer SOL. Also, the neutrals were found to move much slower (velocities ~ 2 – 4 km/sec) in the outer SOL compared to the inner SOL (velocities ~ 4 – 10 km/sec).

Temperatures were determined from the Doppler broadening of the spectral lines and were found to be in the range of ~ 15 – 25 eV for the He^+ ions in the inner and outer SOL's. Much lower temperatures of ~ 2 – 5 eV were indicated for the deuterium atoms in both SOL's. It is observed that the ions flow in the direction of the plasma current in both inner and outer mid-plane SOL regions, as do the neutrals in the inner SOL. Unexpectedly, the neutrals flow in the opposite direction in the outer mid-plane SOL. $E_r \times B_\theta$ drifts seemed to be a likely candidate for driving the flows.

These results were presented at an APS Division of Plasma Physics meeting and published in Physics of Plasmas [1].

MARYLAND CENTRIFUGAL EXPERIMENT ("MCX")

Integrated Spectroscopy in the Visible Region.

Later, the MIT/Alcator procedures described above based upon visible spectroscopy were transferred to the new Maryland centrifugal experiment (MCX). In this device [2,3], enhanced confinement along axial magnetic field lines in a solenoid with mirror end fields is obtained by applying a radial electric field between a central conductor and the outer wall, thereby generating azimuthal $\overline{E}_r \times \overline{B}_z$ forces. This configuration promises reduced end losses, shear stabilization and viscous heating. Integrated intensity observations along a chord in the plasma of the Doppler shift of spectral lines yielded a confirmation of rotation of the plasma, with azimuthal velocities ranging from 20 to 100 km/sec for carbon impurities in increasing ionization states and 10 km/sec for hydrogen atoms. Also obtained from thermal Doppler line broadening were impurity-ion temperatures of 10-40 eV, and hydrogen-atom temperatures of 5-10 eV. An electron temperature of ~15 eV was inferred from relative line intensities of different ionic species of carbon.

These results were presented at the APS Division of Plasma Physics meeting and published in Physics of Plasmas [4]. (Appendix A)

Spectroscopy in the Vacuum Ultraviolet Region.

In an effort towards data refinement, and a further understanding of these differences (possibly related to spatial variations) we expanded the hydrogen measurements from the $n \rightarrow 2$ Balmer series in the visible to the $n \rightarrow 1$ Lyman series in the vacuum-ultraviolet (vuv) spectral region. The widths of the lower-n Lyman resonance lines were expected to be enhanced by opacity, decreasing towards higher quantum number along the series, with an associated increase in the depth of view. Such opacity-sensitive measurements can be very useful for comparison with radiative transfer modeling in fusion devices and for determination of the absorber lower (ground) state density.

The results indicated, from opacity on the Lyman series, ~6% atomic hydrogen coexisting with protons, electrons and carbon-impurity ions in a plasma region where the temperature is ~15 eV. An explanation was offered, based upon charge exchange of entering cold hydrogen atoms with plasma protons, followed by collisional excitation and radiative decay.

These results were presented at the APS Division of Plasma Physics meeting and published in Physics of Plasmas [5]. (Appendix B)

Space-Resolved Visible Spectroscopy.

Our most recent experiments on MCX incorporated the high resolution spectrograph used in the Alcator experiments described above, which included five channels of fiber-optic viewing for spatial resolution. Viewing was such that five circular layers were defined. The data are currently being inverted and modeled to obtain radial distributions of velocity and density which may indicate the degree of shear present for stabilization. It is anticipated that this analysis will be complete for presentation at the 2005 APS/DPP meeting in Denver, CO in November 2005 and will be published in an appropriate journal.

REFERENCES

1. "Measurements of Ion and Neutral Atom Flows and Temperatures in the Inner and Outer Mid-Plane Scrape-Off Layers of the Alcator C-Mod Tokamak", by J. Ghosh, H. Griem, R. Elton, J. Terry, E. Marmar, B. Lopschultz, B. LaBombard, J.E. Rice and J.L. Weaver, Phys. of Plasmas **11**, 1033 (2004).

2. R.F. Ellis, A.B. Hassam, S. Messer, and B.R. Osborn, Phys. of Plasmas **8**, 2057 (2001).

3. "Steady supersonically rotating plasmas in the Maryland Centrifugal Experiment", R. Ellis, A. Case, R.C. Elton, J. Ghosh, H.R. Griem, A.B. Hassam, R. Lunsford, S. Messer and C. Teodorescu, Physics of Plasmas **12**, 055704 (2005).

4. "Spectroscopic measurements of plasma rotation and ion and neutral atom temperatures in the Maryland Centrifugal Experiment", J. Ghosh, R.C. Elton, H.R. Griem, A. Case, R. Ellis, A.B. Hassam, S. Messer and C. Teodorescu, Physics of Plasmas **11**, 3813 (2004). See Appendix A here.

5. "Vacuum Ultraviolet measurements of hydrogen resonance lines in the Maryland Centrifugal Experiment (MCX)" by J. Ghosh, R. Elton, H. Griem, C. Teodorescu, A. Case and R. Ellis, Physics of Plasmas **12**, 034501 (2005).). See Appendix B here.

Appendix A

~~Joy: Do you have to show your email address in this? PAC numbers?~~

Spectroscopic measurements of plasma rotation and ion and neutral atom temperatures in the Maryland Centrifugal Experiment (MCX)*

J. Ghosh, R. C. Elton, H. R. Griem, A. Case, R. Ellis, A. B. Hassam, S. Messer, and C. Teodorescu.
Institute for Research in Electronics and Applied Physics
University of Maryland, College Park, MD 20742

ABSTRACT

In initial spectroscopic measurements on the Maryland Centrifugal Experiment (MCX), rotation velocities and directions for C^+, C^{2+}, C^{3+} and N^+ ions and neutral hydrogen atoms have been obtained from the Doppler shifts of visible spectral lines. Ion and neutral temperatures have also been determined from Doppler broadening. Different rotation velocities and temperatures are observed for the different species. The direction of rotation is found to be consistent with the predicted ~~$E_r \times B_z$~~ $\overline{E_r} \times \overline{B_z}$ direction; and it reverses with the direction of the magnetic field. The magnitudes of the rotation velocities were of the same order as estimated from the ~~plasma stored energy~~applied voltage and magnetic field. For the C^+, C^{2+} and C^{3+} species, rotation velocities of 20 – 30 km/sec, 40 – 70 km/sec and 60 – 100 km/sec are observed, respectively. The corresponding temperatures are 10 – 12 eV, 20 – 40 eV and 25 – 40 eV. Neutral hydrogen atoms are observed to rotate with velocities ~10 km/sec and with temperatures ~ 5 – 10 eV. These ion velocities and temperatures correspond to sonic Mach numbers (u_φ / c_s) ranging from 1 – 2. Variations of rotation velocities and temperatures with axial magnetic field, radial electric field, and mirror ratio are described. An electron temperature of ≈ 15 eV is inferred from the relative line intensities from different ionic species of carbon, which is consistent with the lack of observable C^{4+} emission.

I. INTRODUCTION

Centrifugal confinement[1] of plasma is being tested in the Maryland Centrifugal Experiment (MCX). The basic idea is to rotate a plasma supersonically and utilize the centrifugal forces generated from the rotation, in conjunction with the magnetic field, to effect confinement of plasmas along the axial magnetic field lines [1 – 6]. These high-speed rotations offer several improvements over standard mirror machines, such as reducing the end losses. Further, the shear in the rotation helps in breaking up convective cells and providing stability against typical plasma instabilities[5]. Viscous heating is predicted[3, 4, 6] to be sufficient to heat the plasma to fusion temperatures in a full-scale device. Hence, with several conditional advantages such as superior cross-field confinement, no disruptions, steady state operation and a very simple coil configuration, this confinement scheme ~~may be scalable to a fusion reactor~~is of interest as a possible fusion device.

Rotating plasmas in MCX are created by applying a radial electric field in~~to~~ a magnetic geometry of a solenoid with axisymmetric mirror end fields. The Lorentz force drives the plasma to rotate in the azimuthal direction at a velocity $v_\phi = \bar{E} \times \bar{B} / B^2 = (E_r / B_z)\hat{\phi}$. ~~Since~~~~As~~ Because the plasma rotation is of primary importance to this concept of centrifugal confinement, we report in this paper the measurement of the ion and neutral rotation velocities as well as the direction of rotation and temperatures achieved to date, using a high-resolution visible spectrograph with temporal resolution. Line emissions from different sections of the MCX plasma were collected; and the rotation velocities and the temperatures of ion and neutrals were determined from the Doppler shift and broadening of the emission lines, respectively. As the use of electrical (Langmuir) probes is difficult in such machines due to the presence of strong electric fields, the spectroscopic techniques provide the most accurate measurements of rotation velocities and temperatures. In the following section we describe briefly the MCX machine, the experimental set-up and spectrometer

characteristics, followed by experimental results in Section III. Section IV contains a discussion and summary.

II. EXPERIMENTAL SET-UP

A cut-away view of the MCX machine in Fig. 1 shows the design and positioning of the MCX vacuum vessel, including the core, the mid-plane coils and the coils near either end. Also visible are the insulating discs just outside the end coils. The diameter of the vacuum vessel is 55 cm at the horizontal mid-plane, with a 326 cm length between the two insulators which intersect the magnetic field lines outside the mirror planes. The core is made up of a stainless steel tube with an outer diameter of 4.83 cm. The radial electric field is generated by applying high-voltage between the central core and the vacuum vessel wall. Typical operation is with a mid-plane magnetic field of 0.2 Tesla and a mirror magnetic field of 1.8 Tesla, i.e., for a mirror ratio of 9. The initial core voltage is – 7 kV. Fill gases at a typical pressure of 5 m Torr include hydrogen, helium and argon.

A cross-section diagram of the MCX vacuum chamber with the central electrode and the collection optics is shown in Fig. 2. The spectrograph viewed the plasma tangentially in the longitudinal mid-plane of the machine. Light from two radial positions, one located below the central electrode at a distance r = 16.5 cm (lower view) and the other above the central electrode also at r = 16.5 cm (upper view), was focused alternately onto the spectrometer slit using lenses L_1 and L_2. Although the lenses were focused to collect light from a very small region in the plasma, the spectrum measured is an integration of the emissions and the plasma conditions along the lines of sight.

A 1.0-m high-resolution Czerny-Turner design stigmatic spectrograph was used to disperse the emission from the plasma. A proximity focused, intensified, ~~m~~M~~icro Channel channel Plate plate (MCP) intensified~~ linear diode array was used to record the emission. The size of detector elements (pixels) was 25 μm (wavelength direction) by 2.5 mm (slit direction), with 900 active elements. A 600-grooves/mm grating provided a reciprocal dispersion near 600 nm in first order of 0.036 nm/pixel. This provided a 32-nm

coverage of the spectrum. The instrumental line width was limited by the detector resolution and was measured to be ≤ 3-pixels (75 μm) using a 50-μm entrance slit width, for a spectral resolution of 0.11 nm. Spectral lamps were employed for wavelength calibration. The D_α spectral line of deuterium at 656.10 nm and two Hg I lines (576.96 nm and 579.06 nm) were used. The time-gated intensifier provided exposures varying from 100 μsec to 2 ms. The read-out time (~ 25 ms) of the detector limits the number of scans in a single discharge (typical pulse length ~ 3 ms) to a single scan.

III. EXPERIMENTAL RESULTS

Data from all discharges reported in this paper are with negative E_r, i.e. the central core is biased negatively with respect to the vacuum vessel and the electric field is directed towards the central core. With the axial magnetic field B_z going into the paper, it is evident from Fig. 2 that the $\bar{E}\times\bar{B}$ rotation of the plasma is in the clockwise direction. This geometry and the configurations of the electric and magnetic fields, with the spectrometer placed on the right hand side of the machine (as shown), implies that line emissions from particles will be red-shifted when observed from the lower view and blue-shifted when observed from the upper view.

A. Methods for obtaining rotational velocities and temperatures

The directed motion of the radiating particles affects the measured line wavelength, because the energy of the transition is Doppler shifted by an amount proportional to the velocity along the line of sight. The relation between the shift of the central wavelength in the rest frame, $\delta\lambda_f$, and the flow velocity, v, is given by

$$\delta\lambda_f / \lambda_0 = (\mathrm{v}/c)\times\cos\theta, \qquad (1)$$

Field Code Changed

where λ_0 is the wavelength of the species in the rest frame, c is the speed of light and θ is the angle between the line of sight and the direction of the flow.

If there exists also random thermal motion, it will produce a broadening of the line shape. The relation between the FWHM (full width at half maximum intensity) of a Doppler broadened line $\delta\lambda_D$ and the temperature of the species which emits the radiation is given by

$$\delta\lambda_D = 2\lambda_0\sqrt{2kT\ln 2/Mc^2}\,, \qquad (2)$$

where M and c are the mass of the species and speed of light, respectively. The wavelength of the species in the rest frame is λ_0. We used the Doppler broadening of the measured line profiles to estimate the ion and atom temperatures, T, of the species.

Field Code Changed

B. Sample Results

Figure 3 shows raw spectral data for different charge states of carbon and nitrogen (see Table 1 for the wavelengths) observed from the lower view in a single MCX discharge (mirror ratio = 9, applied voltage = -7 kV, fill pressure = 5 mTorr and mid-plane magnetic field = 1 kGauss). A Hg I calibration line (576.96 nm) is also shown. A typical H_α profile (at 656.28 nm) as observed from the lower view is illustrated in Fig. 4. The curve through the experimental points is the result of a numerical fit to the experimental data. For the typical parameters of the MCX plasma (applied electric and magnetic fields), the Stark -and Zeeman-effects have negligible influence on the observed line shapes. The Stark broadening is less than 0.2% (at an electron density $\approx 1 \times 10^{20}$ m^{-3}) for the C II line at a wavelength~~)~~ of ~~(~~589 nm~~)~~ compared to the Doppler broadening and it will be even less for C III and C IV according to the Z-scaling[7]. Also, t~~T~~he Zeeman splitting is less than 4% (at a mid-plane magnetic field = 0.2 Tesla). -Hence, ~~a Gaussian~~ line shape has been used to fit all of the experimental Doppler broadening data. The plot parameters are obtained by nonlinear least square fits to the corresponding experimental line shapes to determine the numerical wavelength shifts and widths. The fitted line profiles have been de-convolved using the instrumental functions to calculate the actual broadening. Errors in the deduced parameters mainly originate from ambiguities in the

numerical fits, which in turn depend on the quality of the spectrum (purity and signal-to-noise ratio). The application of χ^2 minimization to the modeling of observations with high signal-to-noise ratios can yield highly-precise values of the central wavelength. For the data presented in this paper an error estimate of ±0.1 pixels, which corresponds to ±0.0036 nm in wavelength for each line center, has been used.

C. Rotation velocities and ion and neutral temperatures

Figure 5 shows the rotation velocity of charge states of different species (C^{3+}, C^{2+}, C^{+}, H^{0}, N^{+}) observed from the red shift (0.02 – 0.14 nm) of spectral lines for the lower view for different (reproducible) MCX discharges (mirror ratio = 9, applied voltage = -7 kV, fill pressure = 5 mTorr and mid-plane magnetic field = 1 kG). As suggested by Fig. 5, the higher charge states rotate faster than the lower ones or the neutral hydrogen. Furthermore, a comparison of the emissions from higher ionization states, which come from hotter regions of the plasma and rotate with higher velocities compared to lower ionization states, that from colder regions, indicates that a large velocity shear exists in the MCX plasma. This result is quite consistent with earlier theoretical investigations[8] ~~by Lehnert[7] Lehnert[8] and earlier~~ and experiments[9,10]. ~~by Bergstrom[8] Bergstrom[9] and Lehnert[9] Lehnert[10].~~ The observation of neutral hydrogen atoms rotating at much lower velocities also agrees with theory[7]{is this really the correct reference?}, which predicts that the interior of the plasma should be screened from neutrals.

The observed line widths (FWHM) of the emissions ranged from 0.11 to 0.14 nm in the parameter range shown in Fig. 5, and result in temperatures ranging from 20 – 25 eV for C^{3+} and C^{2+} ions, 10 – 12 eV for C^{+} and N^{+} ions, and 5 – 10 eV for neutral hydrogen.

Figure 6(a, b) shows the variation of rotation velocities and ion temperatures inferred from shifts and line broadening of C IV, C III, and CII line emissions as a function of applied axial magnetic field at the mid-plane of the machine. The data points are obtained from ~~different~~separate MCX discharges (all for mirror ratio = 9, fill pressure

= 5 mTorr and applied bias voltage = -7 kV) with at least three shots with the same set of parameters. ~~Furthermore,~~ This figure shows that ~~t~~he rotation velocities increase with increasing axial magnetic field for the C^{3+} and C^{2+} ions ~~(graphs to appear in a subsequent paper[10])~~. Rotation velocities of ~ 100 km/sec and ~ 70 km/sec are observed for the C^{3+} and C^{2+} ions, respectively, for an applied mid-plane magnetic field of ~ 2 kG. Ion temperatures for C^{3+} and C^{2+} also increase monotonically with the increase in the mid-plane magnetic field[10]. However, the velocity and the temperature of C^{+} ions remain almost constant and do not vary greatly with magnetic field[10]. The increasing trend of the rotation velocities with the mid-plane magnetic field is also consistent with the indirect measurements of the rotation velocities derived from the measured voltage across the plasma and mid-plane magnetic fields. The open down-triangles in the Fig. 6a represent the velocity calculated from the measured voltage across the plasma and mid-plane magnetic fields.

Although the basic magnetic configuration of the MCX machine is that of a mirror machine, spectroscopic data do not indicate ~~the~~any significant dependence of mirror ratio ~~does not appear to play an important role~~ ~~i~~on ~~the~~ plasma dynamics in the central mid-plane of this centrifugally confined plasma.~~,~~ ~~as~~ The mirror ratio has been varied by~~determined by~~ changing the mirror (end) magnetic fields while keeping the mid-plane magnetic field constant at 1kG. Also, the rotation velocities and ion temperatures inferred from shifts and line broadening of C III line emissions remain constant with increasing bias voltage applied to the central electrode for the discharges presented in this paper with fixed external circuitry of the MCX machine.

D. Confirmation of Rotation

Plasma in MCX is expected to rotate about the central electrode. Observing moving plasma particles from the lower view does not alone confirm such a circulation of the plasma. To be certain, we need to observe the plasma from the upper view, moving in a direction opposite to that from the lower view, i.e., towards the slit in Fig. 2. To confirm this circulation of the particles we made measurements at the upper view as well,

above the central electrode. Figure ~~6~~ 7 {there is no caption for Fig. 7}shows the C III line (569.60 nm) from C^{2+} ions observed from both the upper and lower views with the normal direction of the axial magnetic field B_z (going into the paper as shown in Fig. 2) and with a reversed direction of the axial magnetic field, from many, ~~(~~reproducible~~)~~, MCX plasmas (mirror ratio = 9, applied voltage = -7 kV, fill pressure = 5 mTorr and mid-plane magnetic field = 1 kGauss). The dotted vertical lines in the figure represent the unshifted wavelength for the CIII line. This clearly shows that the C^{++} ions are moving away from the spectrometer (spectral lines are red shifted) when observed from the lower port, whereas, the same ions are moving towards the spectrometer (measured spectral lines are blue-shifted) when observed from the upper port (Figs. ~~6a~~ 7a and ~~6b~~7b). These measurements clearly indicate that the MCX plasma is encircling the central electrode in a direction consistent with the $E_r \times B_z$ $\overline{E_r} \times \overline{B_z}$ force. As further proof, we reversed the direction of B_z {no space here between B and z} and observed the CIII line emission reversed (Figs. ~~6c~~ 7c and ~~6d~~7d).

IV. DISCUSSION AND SUMMARY

Analyzing the Doppler shift of line emissions from different ions and neutral hydrogen atoms, we find an increasing rotational velocity with increasing ionization state (Fig. 5) in typical MCX plasmas. The C^{3+} ions rotate with a velocity of ~ 80 km/sec, while the neutral hydrogen atoms rotate at a relatively low velocity. The direction of rotation as well as its magnitude are consistent with the $\overline{E_r} \times \overline{B_z}$ ~~$E_r \times B_z$~~ force on the particles and the rotation velocities calculated from the stored electrostatic energy in the plasma. Ions in the higher ionization state rotate more rapidly than the lower ones, perhaps due to the fact that the emissions from the higher ionization states come from hotter regions of the plasma. This suggests that large velocity shear exists in MCX.

The rotation velocity due to the $\overline{E_r} \times \overline{B_z}$ ~~$\mathbf{E_r \times B_z}$~~ force is given by $v_\phi = \bar{E} \times \bar{B} / B^2 = (E_r / B_z)\hat{\phi}$. Hence, increasing the axial magnetic field B_z should decrease the rotation velocity at constant voltage. However, increasing rotation velocities for C^{2+}

and C^{3+} ions have been observed with increasing axial magnetic fields in the experiments. This may be due to modifications of the potential structures inside the plasma with increasing B_z as obtained in earlier experiments in Q-machines[11].Or, ~~or~~ better confinement due to the higher magnetic fields can lead to higher rotation velocities of C^{2+} and C^{3+} ions. Temperatures of these ions also increase with the increasing magnetic field.

~~Varying the~~ No strong dependence of ~~mirror ratio on~~ does not affect the rotation velocities and temperatures on the mirror ratio in this parameter range of MCX plasma~~, which indicates that the mirror field has a minimal effect on the plasma rotation. Again,~~ has been observed and ~~vary~~variation~~ing~~ of the applied bias voltage ~~in this paramater range~~ also does not ~~change~~ affect these same parameters.~~, which~~ The latter result is consistent with the measured electric field E_r across the plasma, which remains almost constant for different bias voltages with a fixed external circuit.

An electron temperature of ≈ 15 eV is inferred from relative intensities of different ionic species of carbon, as tabulated in Table I. The ionization fractions are obtained from the abundances of the different species of carbon according to the corona equilibrium model described in Ref. 12. This estimate of electron temperature from the corona equilibrium model is consistent with the lack of observable C^{4+} emission in our experiments.

In summary, the rotation velocity and the temperature of C^{3+} for a mid-plane magnetic field of 2 kG correspond to a sonic Mach number (u_φ / c_s) of ~2, which indicates that supersonic rotating plasmas are produced and confined in MCX.

Acknowledgement:

The authors would like to thank J. Rodgers for his help in computer programming for data acquisition.

TABLE I~~1~~: Wavelengths and ionization potentials ~~table~~ for ~~different~~ elements studied.

Spectrum	Rest Wavelength [nm]	Transitions	Ionization Potential
H I	656.28 ~~nm~~	$2p\ ^2P^0 - 3d\ ^2D$	13.597 eV
C II	588.98, ~~nm and~~ 589.16 ~~nm~~	$3d\ ^2D - 4p\ ^2P^0$	24.381 eV
C III	569.59 ~~nm~~	$3p\ ^1P^0 - 3d\ ^1D$	47.881 eV
C IV	580.13, ~~nm and~~ 581.20 ~~nm~~	$3s\ ^2S - 3p\ ^2P^0$	64.490 eV
N II	568.62, ~~nm and~~ 567.96 nm	$3s\ ^3P^0 - 3p\ ^3D$	29.611 eV

REFERENCES

* Supported by DoE.

1) B. Lehnert, Nucl. Fusion **11**, 485 (1971).

2) G. F. Abdrashitov, A. V. Beloborodov, V. I. Volosov, V. V. Kubarev, Y. S. Popov, and Y. N. Yudin, Nucl. Fusion **31**, 1275 (1991).

3) R. F. Ellis, A. B. Hassam, S. Messer, and B. R. Osborn, Phys. Plasmas **8**, 2057 (2001).

4) A. B. Hassam, Comments Plasma Phys. Controlled Fusion **18**, 275 (1997).

5) P. W. Terry, Rev. Mod. Phys. **71**, 109 (2000).

6) B. R. Osborn, R. F. Ellis, and A. B. Hassam, Phys. Plasmas **10**, 2389 (2003).

7) H. R. Griem, Spectral Line Broadening by Plasmas (Academic Press, New York, 1974).

~~7)~~8) B. Lehnert, Arkiv f. Fysik **28**, 205 (1968) and B. Lehnert, Nucl. Fusion **8**, 173 (1968).

~~8)~~9) J. Bergstorm, S. Holmberg, and B. Lehnert, Plasma Physics and Controlled Nuclear Fusion Research, I. A. E. A., vol. **I**, p. 341, Vienna, 1966.

~~9)~~10) B. Lehnert, J. Bergstorm, S. Holmberg, and B. Wilner, Physica Scripta. Vol. **1**, 39 (1970).

~~10) R. Ellis et al., manuscript in preparation (2004).~~

~~10)~~11) M. Koepke, private communication (2003).

~~11)~~12) P. Mazzotta, G. Mazzitelli, S. Colafrancesco, and N. Vittorio, Astron. Astrophys. Suppl. Ser. **133**, 403 (1998).

Formatted: Bullets and Numbering

FIGURE CAPTIONS

Formatted: Normal

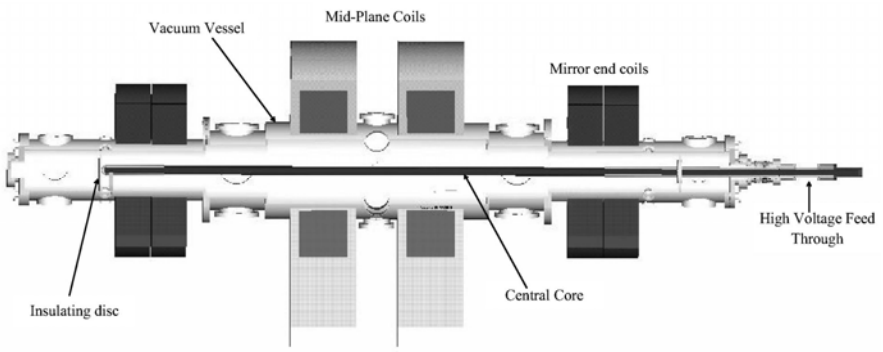

Formatted: Normal

Figure 1. A cut-away view of the MCX machine. The view shows the design and positioning of the MCX vacuum vessel, including the central core with the high voltage feed-through on the right, the mirror end and mid-plane magnetic coils and the insulating disc just outside the mirror end magnetic coils.

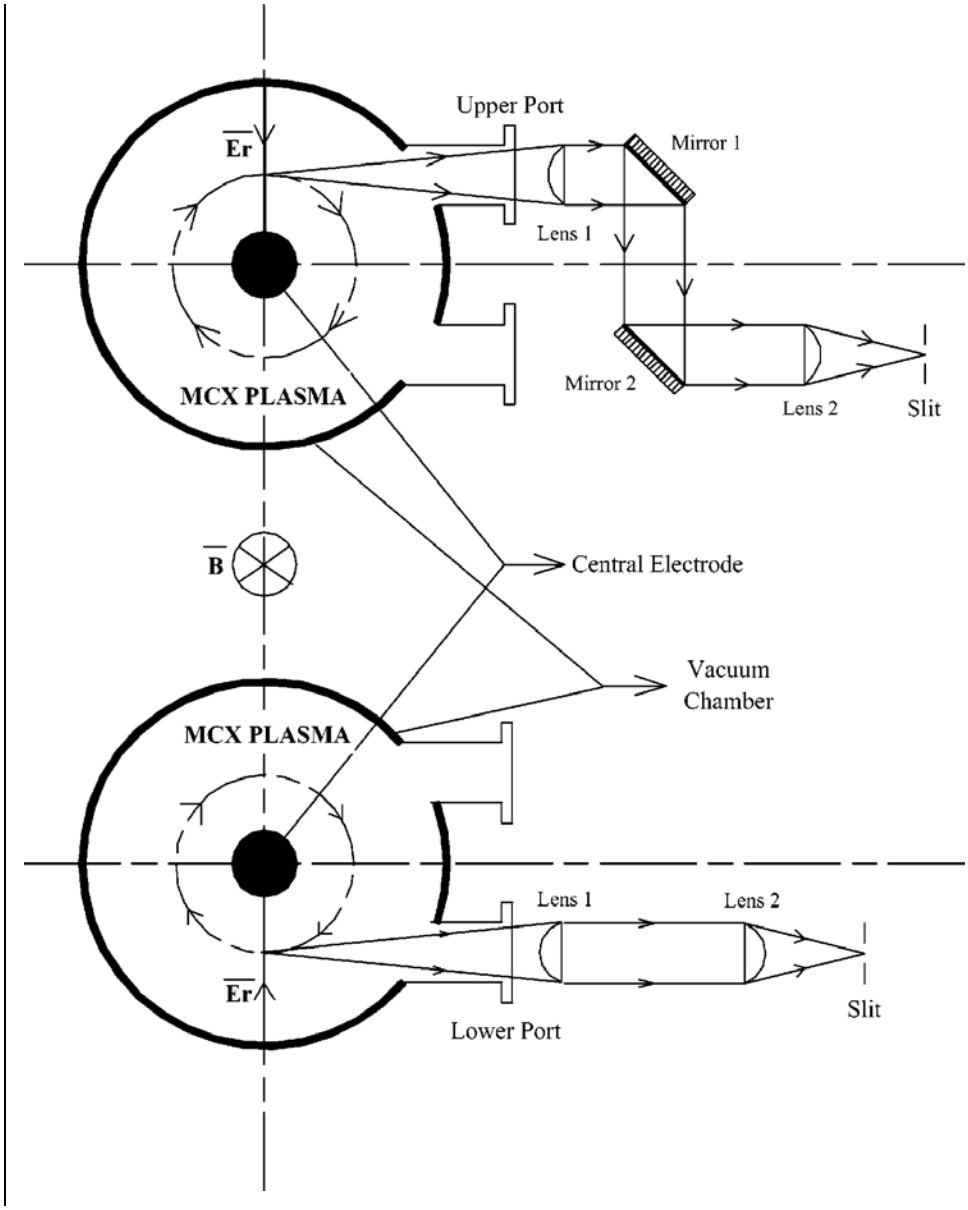

Figure 2. A cross-section of the MCX vacuum chamber with central electrode showing the viewing geometry and the collection optics. Also shown are the direction of applied electric and magnetic fields and the direction of rotation due to the ~~$E_r \times B_z$~~ $\overline{E_r} \times \overline{B_z}$ force.

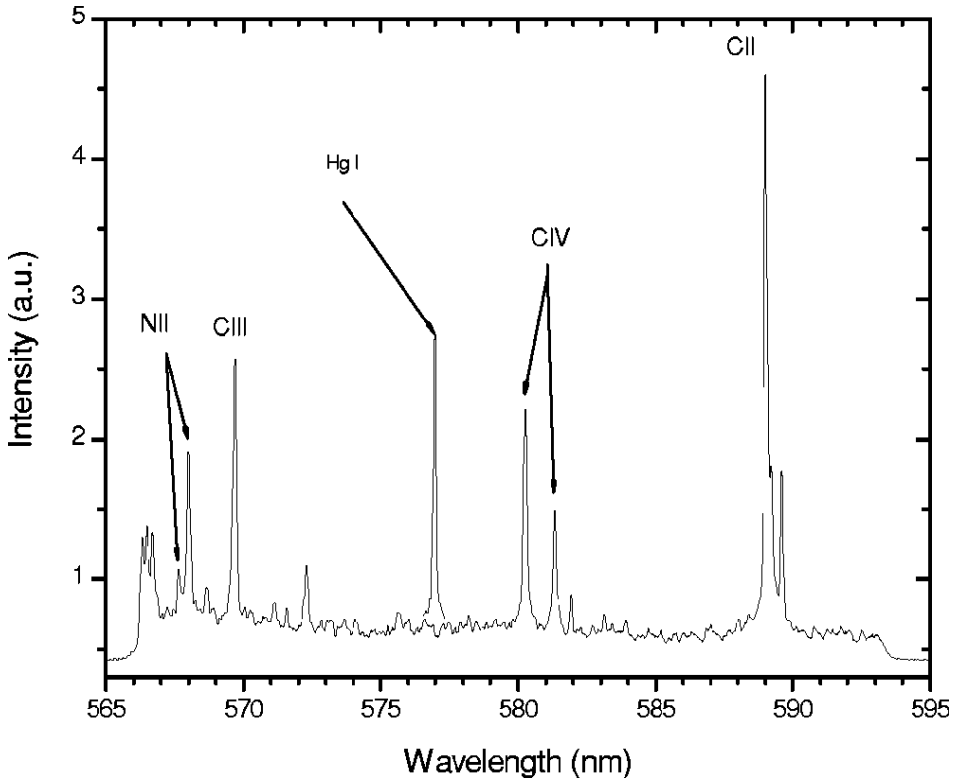

Figure 3. Raw spectral data for different charge states of carbon and nitrogen observed from the lower view in a single MCX discharge (mirror ratio = 9, applied voltage = -7 kV, fill pressure = 5 mTorr and mid-plane magnetic field = 1 kGauss). A Hg I calibration line (576.96 nm) is also shown.

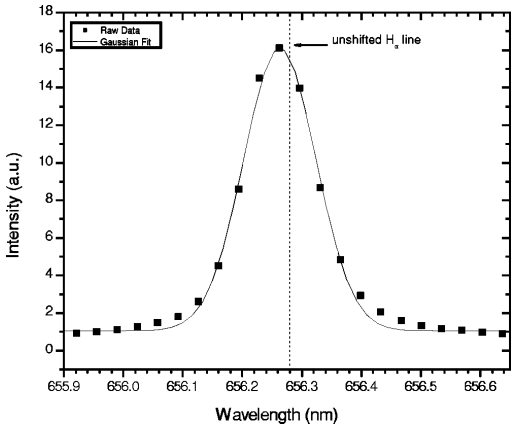

Figure 4. A typical H_α profile (at 656.28 nm) as observed from the lower view.

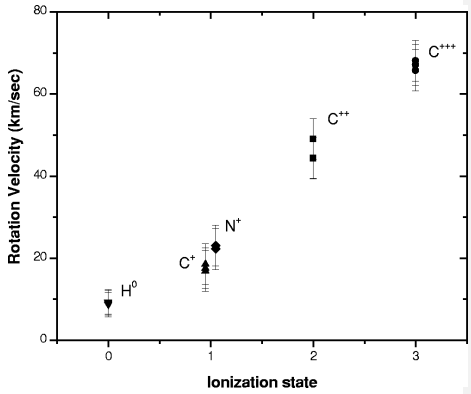

Figure 5. Rotation velocities of different species (C^{3+}, C^{2+}, C^{+}, H^{0}, N^{+}) observed from the lower view for different (reproducible) MCX discharges (mirror ratio = 9, applied voltage = -7 kV, fill pressure = 5 mTorr and mid-plane magnetic field = 1 kG). To avoid overlapping, C^{+}, N^{+} data are deliberately separated from each other.

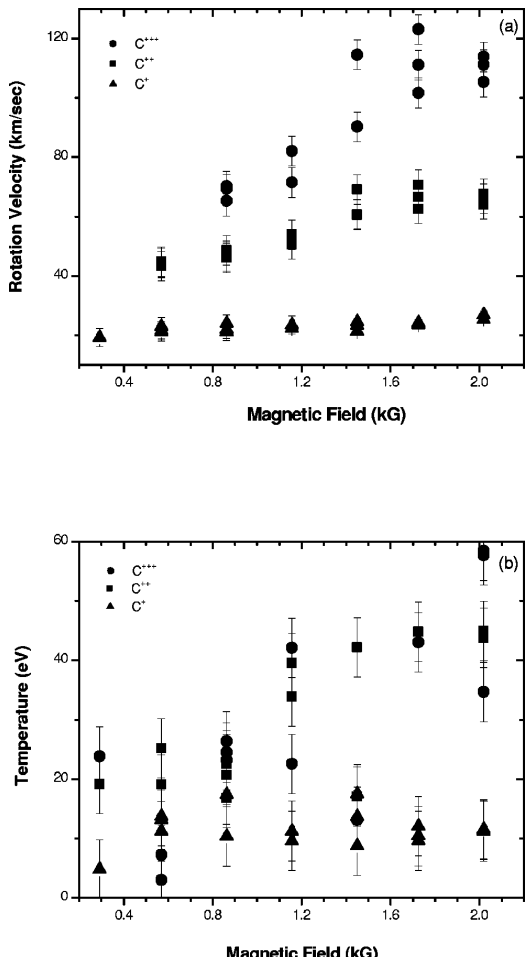

Figure 6. C III line (569.60 nm) emission from C^{2+} ions observed from both the upper (b, d) and lower views (a, c) with normal (a, b) (going into the paper as shown in figure 2) and reversed (b, c) direction of the axial magnetic field, B_z, from many reproducible MCX plasmas (mirror ratio = 9, applied voltage = -7 kV, fill pressure = 5 mTorr and mid-plane magnetic field = 1 kGauss).

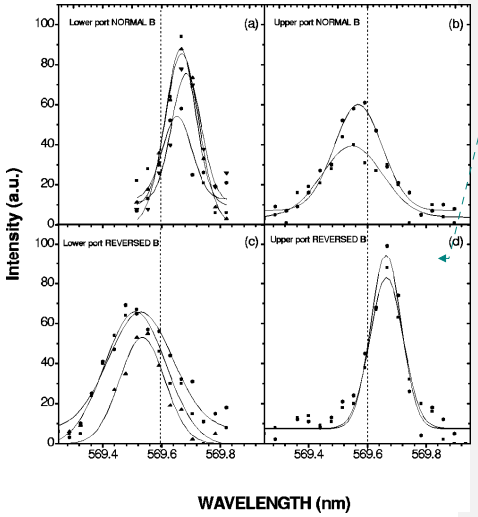

Formatted: Centered

FIG. 7. C III line (569.60 nm) emission from C^{2+} ions observed from both the upper (b), (d) and lower views (a), (c) from many reproducible MCX plasmas (mirror ratio=9, applied voltage=−7 kV, fill pressure=5 mTorr, and midplane magnetic field=1 kG). Graphs (a), (b): normal direction of the axial magnetic field, B_z, (going into the paper as shown in Fig. 2) and (b), (c) reversed direction of the axial magnetic field.

~~Figure 7. NEED CAPTION HERE~~

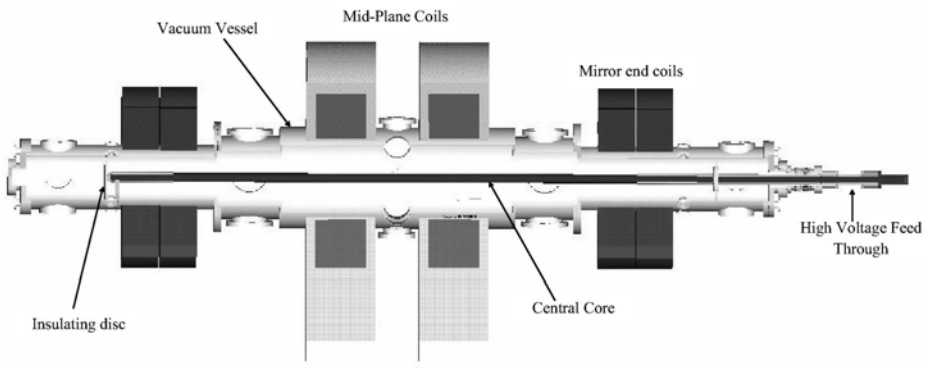

Figure 1

Formatted: Centered

Appendix B

Vacuum ultraviolet measurements on hydrogen resonance lines in the Maryland Centrifugal Experiment (MCX)

J. Ghosh, R. Elton, H. Griem, C. Teodorescu, A. Case, and R. Ellis

Institute for Research in Electronics and Applied Physics
University of Maryland, College Park, MD 20742

Abstract

Extended spectroscopic measurements of hydrogen emission into the vacuum ultraviolet region on the Maryland Centrifugal Experiment (MCX) indicate, from opacity on the Lyman series, ~6% atomic hydrogen coexisting with protons, electrons and carbon-impurity ions in a plasma region where the temperature is ~15 eV. An explanation is offered, based upon charge exchange of entering cold hydrogen atoms with plasma protons, followed by collisional excitation and radiative decay.

INTRODUCTION

In a previous paper [1], visible spectroscopy was used as a diagnostic on the Maryland centrifugal experiment (MCX). In this device [2], enhanced confinement along axial magnetic field lines in a solenoid with mirror end fields is sought by applying a radial electric field between a central conductor and the outer wall, thereby generating azimuthal $\overline{E}_r \times \overline{B}_z$ forces. This configuration offers reduced end losses, shear stabilization [3] and viscous heating [4]. Observations along a chord in the plasma of the Doppler shift of spectral lines yielded a confirmation of rotation of the plasma, with azimuthal velocities ranging from 20 to 100 km/sec for carbon impurities in increasing ionization states and 10 km/sec for hydrogen atoms. Also obtained from thermal Doppler line broadening were impurity-ion temperatures of 10-40 eV, and hydrogen-atom

temperatures of 5-10 eV. An electron temperature of ~15 eV was inferred from relative line intensities of different ionic species of carbon.

In an effort towards data refinement, and a further understanding of these differences (possibly related to spatial variations) we expanded the hydrogen measurements from the n→2 Balmer series in the visible to the n→1 Lyman series in the vacuum-ultraviolet (vuv) spectral region. The widths of the lower-n Lyman resonance lines are expected to be enhanced by opacity, decreasing towards higher quantum number along the series, with an associated increase in the depth of view. Such opacity-sensitive measurements can be very useful for comparison with radiative transfer modeling in fusion devices and, as herein, for determination of the absorber lower (ground) state density.

EXPERIMENTAL DETAILS

Plasma Device

In the MCX, the diameter of the vacuum vessel is 55 cm at the mid-plane, with separations of 250 cm between the two mirror coils and 330 cm between the two insulators which intersect the magnetic field lines outside the mirror planes. The axial core consists of a hollow stainless steel tube with an outer diameter of 4.8 cm. Typical operation for these experiments was with a mid-plane magnetic field of 0.2 Tesla (2 kG) and a mirror magnetic field of 1.8 Tesla (18 kG), for a mirror ratio of 9. The initial potential between the core and the wall was –7 kV. The hydrogen gas fill was at a pressure of 5 mTorr ($3x10^{14}$ atoms/cm^3). A typical shot lasted ~7 ms. The plasma was found to exist in two distinct modes. The first "high-rotation" mode lasted ~2.5-to-3 ms (depending upon the magnetic field, the radial electric field and the external resistance of the circuit) and was characterized by low radial currents, high rotational velocities and good confinement times, but also by an abundance of impurity lines. The presence of such impurities presumably resulted from a release at the wall, at the central conductor

and at the end insulators. The spontaneous onset of the second "ordinary-rotation" mode at ~3 ms after breakdown was accompanied by a greatly-reduced impurity level and improved signal-to-noise ratio for the higher-n Lyman-series spectral lines. Hence, for most of the measurements reported here, the detector was gated on for a time of 3-7 ms.

Vacuum Ultraviolet Spectroscopy

For the vacuum ultraviolet spectroscopic measurements, the plasma was viewed along a chord 17.5 cm from the axis of symmetry, as indicated in Fig. 1. A 1-meter, f/10, normal incidence monochromator equipped with a 1200 grooves/mm grating blazed at 2.7^{o} (80-nm Littrow wavelength) was used in first order. It was custom-coated with magnesium fluoride for maximum efficiency in the 93.0-121.6 nm wavelength range of interest. The reciprocal linear dispersion of the spectrograph was 0.83 nm/mm at the focal plane, where an evaporated layer of Liumogen [5] phosphor served to convert the vacuum ultraviolet radiation into broadband fluorescent emission at a wavelength centered at 530 nm. The image at this phosphor was focused with a magnification of 2.8-times onto a microchannel-plate-intensified linear diode array with a pixel size of 25 μm. The resulting dispersion at the detector was 135 px/nm, as measured directly. With a total of 900 pixels, the overall wavelength coverage was 6.7 nm.

An instrumental resolution of 6 pixels or 0.044 nm was determined by combining numerical best-fittings of two Gaussian profiles to two C II impurity lines at 103.634 and 103.702 nm, i.e., separated by 0.068 nm. This resolution is consistent with the width of a reabsorption dip appearing (particularly when viewing in the early phase) near the center of the Lyman-α line of neutral hydrogen at a wavelength of 121.6 nm, as discussed below.

The relative sensitivity of the vacuum ultraviolet spectrograph was determined for the $n \rightarrow 1$ Lyman-series lines at wavelengths between 93.1 nm (n=7) and 102.5 nm (n=3) by comparison with the $n \rightarrow 2$ Balmer-series lines at wavelengths between 397.0 nm (n=7) and 656.3 nm (n=3), which were calibrated using a tungsten lamp as described below.

Here the branching ratios of transition probabilities [6] were used for the comparison. This relative calibration was continued over the series by comparison with a capillary discharge lamp, which was also cross-calibrated with the Balmer series. For the most intense Lyman-α line, a ND = 0.8 neutral-density filter of 16% transmission was added in the fluorescent beam. In order to avoid variations of sensitivity across the phosphor and the detector, each spectral line was recorded at the same location on the phosphor and the detector surfaces by varying the grating angle between shots.

With no focusing lens at the entrance of the vuv spectrograph, the lateral extent of the plasma viewed at the midplane was 14 cm. The view was aperture-limited by the porthole through the vacuum tank (see Fig. 1). As such, the view was of the more dense portion of the ~19 cm radial extent of the plasma. As illustrated in Fig. 1, this wide view was also used with the visible spectrometry described next. An alternate focused view in the visible was also used for a comparison with the previous measurements [1]. With a possible exception at the center of the optically-thick vuv lines, the emissions measured were an average along the chordal line of sight.

Visible Spectrometry

Supporting visible spectroscopy evolved from previous measurements [1] of the Balmer-series lines, with the addition of a measurement of electron density from Stark broadening . In the present case, observations were possible for lines with wavelengths from 656.3 nm for n=3 to 379.8 nm for n=10. The lines were dispersed using a 1.0-m Czerny-Turner stigmatic spectrograph. The plasma was viewed simultaneously through a quartz fiber along a similar axis as that for the vacuum-uv spectroscopy, except at the upper port (see Fig. 1). Initially a 1-cm diameter focusing lens was used to reproduce the earlier [1] data with a viewing aperture limited to $\lesssim$5 mm in the plasma. However, in an effort to better compare the visible and vuv data, the visible spectra were recorded here without a focusing lens (as shown in Fig. 1) in order to provide essentially the same wide field of view as that of the vuv spectrometer.

A CCD camera, intensified and gated by a lens-coupled microchannel plate, was used to record the visible emission. The size of each detector element (pixel) was 25 μm, with 748 active elements in the wavelength direction. A 1200-grooves/mm grating provided a reciprocal dispersion near 600 nm in first order of 0.0178 nm/pixel. This resulted in a 11.8 nm coverage of the spectrum. The instrumental line width was limited by the detector resolution and was measured to be 3-pixels (75 μm) using a 50-μm entrance slit width, for a spectral resolution of 0.053 nm. The effect of the instrumental line broadening was included by convoluting a representative Lorentzian profile with a simulated Gaussian profile for the Doppler-broadened plasma emission and achieving a best fit. The relative sensitivity of the spectrograph was determined by calibration with a tungsten ribbon standard lamp, as mentioned above. This was possible over a wavelength range from 656.3 nm at Balmer-α (n=3) to 397.0 nm at Balmer-ε (n=7), as limited by the output lamp. This provided relative Balmer line intensities useful in our interpretations which follow.

RESULTS

The measured n→1 Lyman series full widths at half maximum for n=2 to 8 (Lyman-α to -ζ) are listed as w_m in column 4 of Table 1, with an estimated accuracy varying from ±15% for Lyman-α and ±20% for Lyman-ζ, and are found to be approximately the equal. In all cases they exceed the value for the instrumental width of 0.044 nm given above and included in column 5 of Table 1 for comparison. Such similar widths, when the Doppler broadening is decreasing for the high-n lines (column 6), can be understood by an increase in Stark broadening along the series (column 7 and references shown). Also, opacity broadening is more important on the lower-n lines, which have greater line strengths [6] and therefore opacity τ, as shown in column 8. Also, while the most intense Lyman-α line was relatively free from underlying impurity contributions, the increasingly less intense recorded spectra for the higher-n lines included significant narrow-band noise, originating from impurity lines from carbon, oxygen and metals such as copper and nickel, which affected somewhat the fitting to the observed widths.

In order to better understand the processes responsible for the observed Lyman line data, especially concerning opacity, a series of best-fit convolutions were performed for each line in the series, with the requirement that they be self-consistent within the series. Another requirement was that the results be consistent with those from the Balmer series. In fact, the widths of the higher members of the Balmer series were significantly larger than could be explained by a thermal Doppler effect convoluted with an instrument function, and were used to derive an electron density of $N_e=(7.7\pm0.8)10^{14}$ cm^{-3}, based upon computations for both n=5 [7] and n=6 [8,9] and an experiment [10] for n=8. This density is in agreement with an interferometric measurement [11]. It is also considerably larger than the hydrogen-atom fill density of $3x10^{14}$ cm^{-3}.

Table 1. Measured and calculated parameters and vuv line widths (in nm).

Lyman-	n	λ [nm]	w_m[a]	w_{ins}	w_D	w_{Stk}	[Ref.]	τ[b]
α	2	121.57	0.082	0.044	0.036	0.00090	[7]	20
β	3	102.57	0.089	0.044	0.031	0.0044	[7,8,9]	3.1
γ	4	97.25	0.112	0.044	0.029	0.0081	[7]	1.1
δ	5	94.97	0.122	0.044	0.028	0.013	[8,9]	0.5
ε	6	93.78	0.111	0.044	0.028	0.019	[$\propto n^2$]	0.29
ζ	7	93.07	0.090	0.044	0.028	0.025	[$\propto n^2$]	0.18
ι	8	92.62	0.090	0.044	0.028	0.033	[$\propto n^2$]	0.12

[a]measured widths ±15-20%;

[b]for d = 30 cm, T_H = 15 eV, N_H = 4.6 x 10^{13} cm^{-3} = (0.06) N_e

The n=4 to n=1 Lyman-γ line was selected as a beginning of the vuv analysis, because it was relatively unaffected by both Stark broadening and opacity (see Table 1). A Gaussian profile of width 0.029 nm simulating the Doppler-broadened plasma emission was convoluted with a 0.044-nm wide Lorentzian instrument function to give the best fit to the measurements. Actually this Doppler width was adjusted also for a best fit to the profile of the Lyman-δ line, the last in the series for which Stark calculations

[8,9] were available, and then on to the higher-n lines by extrapolating the theoretical Stark widths as n^2 (see Table 1). The fact that these higher-n Lyman lines can be fitted with Stark broadening, which is sensitive to electron density, supports our measurement of that density from the higher Balmer lines, as described above. The best Doppler fit to the Lyman-γ (and higher-n) lines corresponds to a hydrogen temperature of $T_H \approx 15$ eV,. This new and increased temperature value is consistent [1] both with a measured ion temperature of $T_i \approx 10\text{-}12$ eV for C^+ ions and an electron temperature of $T_e \approx 15$ eV, and will be discussed further below.

For the n=2-1 Lyman-α line, the Doppler width scales linearly upward with wavelength to 0.025 nm and clearly would not provide a suitable fit for this intense line, even when convoluted with the instrument function, as shown in Fig. 2. Additional opacity broadening was applied to modify the Doppler profile by using the basic radiative transfer relation $I_{21}(\lambda) \propto 1\text{-}e^{-\tau(\lambda)}$ for a uniform medium. Here $\tau(\lambda)$ represents the opacity, i.e., the product of the line absorption coefficient and the depth of the medium d. As such, $\tau(\lambda)$ varies linearly with the neutral hydrogen density N_H (to be determined), the oscillator strength [6] f =0.416 and the wavelength of the line and inversely with the square root of the hydrogen-atom temperature, along with the Gaussian line shape function [12]. The resulting opacity-broadened Gaussian profile $I_{21}(\lambda)$ was again convoluted with a Lorentzian instrument function. As shown in Fig. 2, it was found that a best overall fit to the data was obtained for a peak opacity of $\tau(\lambda_o) \sim 20$, which leads, for an assumed depth d=30 cm and a measured temperature $T_H = 15$ eV, to $N_H = 4.6 \times 10^{13}$ cm^{-3}, which is 6% of the measured electron density. (The plasma may have a larger radial extent than suggest by the drawing in Fig. 1.)

On some shots, particularly during the early mode following breakdown, the Lyman-α line emitted from the rotating plasma showed a near-central dip, characteristic of absorption in a thin and dense, cold, stationary outer layer near the wall. This dip can be seen in Fig. 2 where a correction to the peak intensity has been applied, based upon a Gaussian best fit to the absorption dip. Small red

shifts of the center of the plasma line emision from that of the reabsorption dip were observed on some shots taken during the early phase of the discharge and were found to be consistent with earlier measurements [1] of a 5.4-times larger (scaling linearly with wavelength) Doppler shift of the Balmer-α line associated with plasma rotation, as indicated in Fig. 1.

For the n=3 to n=1 Lyman-β line, the peak opacity assumed was reduced to 3.1, because of the lower oscillator strength and the shorter wavelength compared to that of the Lyman-α line. No definite central dip associated with the considerably-weaker absorption near the wall was observed. Nevertheless, there was a noticeable enhancement of the calculated width when opacity is included. Also apparent were the contributions of copper and nickel impurity lines, which became more apparent at the rather sharply reduced grating efficiency at wavelengths between the Lyman-α and Lyman-β lines [5].

The existence of hydrogen atoms radiating on Lyman transitions from a plasma at a temperature of $T_H \approx 15$ eV, as encountered here, can occur when cold atoms enter the plasma and undergo symmetrical charge exchange $p + H \leftrightarrow H + p$ with 15 eV protons at a density $N_p = N_e = 7.7 \times 10^{14}$ cm^{-3} . With a cross section of $\sigma_{pH} \approx 3 \times 10^{-15}$ cm^2 (Fig. 3.24 of Ref. 13), the mean free path for entering cold hydrogen atoms to undergo charge exchange is $(N_p \sigma_{pH})^{-1} \approx 2$ cm, with the resulting energetic atoms migrating through the hot plasma and serving as vuv absorbers.

Besides line widths discussed so far, the relative line intensities also are useful in characterizing the plasma. From the measured $n \rightarrow 1$ Lyman-series integrated relative line intensities I_{n1} for n=2 to n=6, corrected for instrumental variations, the reduced populations N_n/g_n ($\pm$50%) were determined using the standard relation $I_{n1} \propto N_n f_n / g_n \lambda_{n1}^3$, where N_n and g_n are population densities and statistical weights for level n, respectively, and λ_{n1} is the wavelength for the $n \rightarrow 1$ transition. Similar results were obtained from the Balmer series for n=3 to n=6, substituting I_{n2} and λ_{n2} above, with an accuracy of $\pm$30%.

The measured values are plotted for both series in Fig. 3 versus n and closely follow a n^{-6} dependence. Such a dependence has been shown (in Fig. 4.5 of Ref. 13) for T_e=11 eV to be characteristic of a "purely-ionizing" plasma at our measured electron density of 7.7×10^{14} cm^{-3}. Here collisional ionization dominates. This is in contrast to a "purely-recombining" plasma where the opposite is true and which also is plotted in Fig. 3 for T_e=11 eV, where N_n/g_n follows (see Fig. 4.13 of Ref. 13) a nearly flat distribution with n. In such a purely-ionizing plasma, ionization proceeds step-wise or "ladder-like" through excitation to higher bound states, followed then by ionization.

SUMMARY

Vacuum ultraviolet spectroscopic measurements on the Lyman resonance lines of atomic hydrogen indicate an opacity of τ_H=20 on the n=2 to n=1 line. Besides being useful in radiative transfer modeling, this has led to an average value along the line of sight for the ground-state hydrogen density ~6% of that of the electrons (as well as protons), determined to be 7.7×10^{14} cm^{-3} from Stark broadening of visible lines and supported by interferometry. The Doppler width giving the best fit to the vuv data indicates a temperature for the hydrogen lines of ~15 eV, in agreement with earlier measurements [1] for ions and electrons. The transient radiating atoms in such a hot plasma are thought to be formed by charge transfer with heated protons.

ACKNOWLEDGEMENTS

The authors would like to thank R. Lunsford for his assistance in the operation of the MCX device. This work was supported by the U.S. Department of Energy.

REFERENCES

1. J. Ghosh, R. C. Elton, H. R. Griem, A. Case, R. Ellis, A. B. Hassam, S. Messer, and C. Teodorescu, Physics of Plasmas **11**, 3813 (2004).

2. R. F. Ellis, A. B. Hassam, S. Messer, and B. R. Osborn, Phys. of Plasmas **8**, 2057 (2001).

3. P. W. Terry, Rev. Mod. Phys. **71**, 109 (2000).

4. B. R. Osborn, R. F. Ellis, and A. B. Hassam, Phys. Plasmas **10**, 2389 (2003).

5. J.A.R. Samson, "Techniques of Vacuum Ultraviolet Spectroscopy", (Pied Publications, Inc., Lincoln, Nebraska, 1967).

6. W. L. Wiese, M.W. Smith and B.M. Glennon, "Atomic Transition Probabilities Volume I, Hydrogen through Neon", NIST Report No. NSRDS-NBS-4, 1966.

7. M. A. Gigosos and V. Cardenoso, J. Phys. B **29**, 4795-4838 (1996).

8. P. Kepple and H. R. Griem, Phys. Rev. **173**, 317 (1968).

9. H. R. Griem, "Spectral Line Broadening by Plasmas" (Academic Press, New York, 1974).

10. B. L. Welch, et al., "Spectral Line Shapes", AIP Conference Proceedings **386**, 113 (1997).

11. C. Teodorescu, A. Case, R. Ellis, A. Hassam, R. Lunsford, S. Messer, C. Cothran and M. Brown, Abstract No. BP1-128, APS 46th Division of Plasma Physics Conference, Savannah, GA, November 2004; Bull. Am. Phys. Soc. __, __(2004).

12. H. R. Griem, "Plasma Spectroscopy" (McGraw-Hill, New York, 1964).

13. T. Fujimoto, "Plasma Spectroscopy" (Oxford Press, UK, 2004).

FIGURES

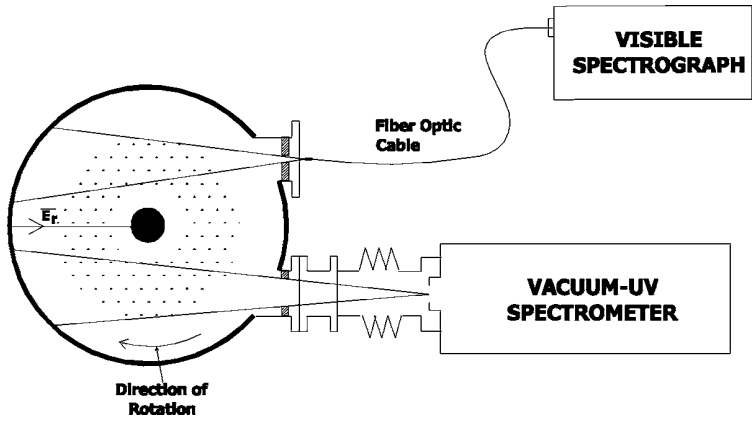

Fig. 1. A cross section schematic (not to scale) of the MCX vacuum chamber with a central electrode. Both the vacuum ultraviolet and visible spectrographs are shown in an unfocused mode, with an ~14-cm radial view at midplane. Implied distinct radial limits for the plasma are symbolic, representing the viewed region of an ~19-cm wide plasma.

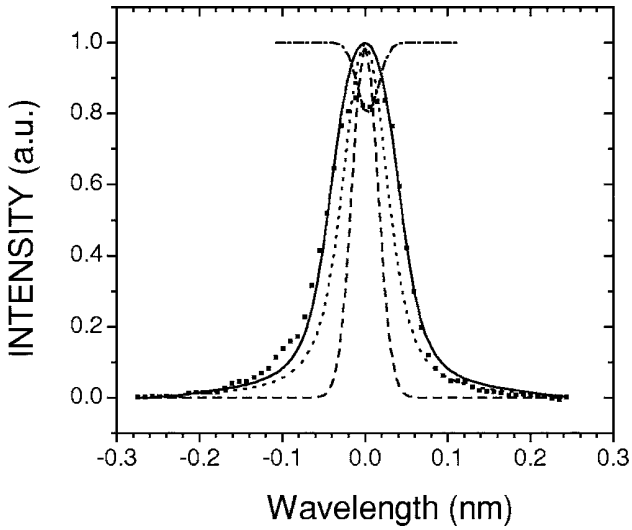

Fig. 2. Best fit for the Lyman-α line of a Gaussian profile (dashed) simulating Doppler broadening, also shown convoluted (dotted) with a 0.044-nm wide Lorentzian instrument function, and finally with opacity added to the initial Gaussian and again convoluted with the instrument function (solid curve). The data is shown as solid squares representing individual pixels. The absorption dip near line center is simulated by a (negative) Gaussian, plotted with alternating dots and dashes.

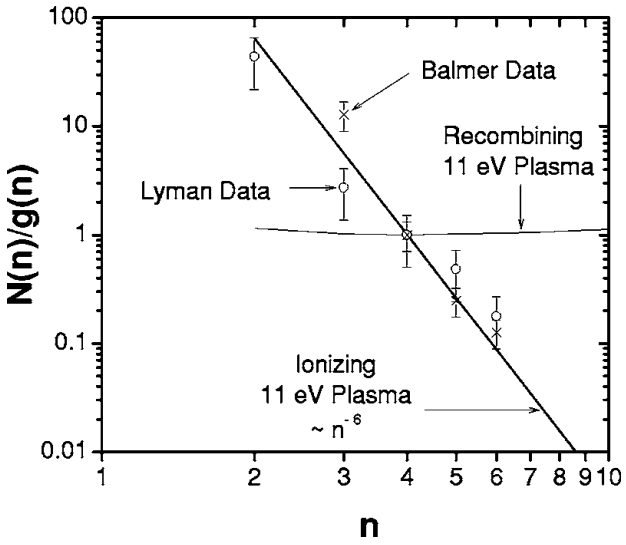

Fig. 3. Reduced population density versus upper quantum level n, showing the characteristic n^{-6} dependence of a purely ionizing plasma. Both modeling [13] (lines) at T_e=11 eV and present data (points) are plotted. Shown for comparison is an approximately constant population predicted for recombination, also at T_e=11 eV. Normalization is to n=4 for clarity.